

1 Bardsey – an island in a strong tidal stream
2 Underestimating coastal tides due to unresolved topography

3
4 J. A. Mattias Green^{1,*} and David T. Pugh²

5
6 ¹ School of Ocean Sciences, Bangor University, Menai Bridge, UK

7 ² National Oceanography Centre, Joseph Proudman Building, Liverpool, UK

8 * Corresponding author: Dr Mattias Green, m.green@bangor.ac.uk
9

10
11
12 **Abstract**

13 Bardsey Island is located at the western end of the Llŷn Peninsula in north-west Wales. Separated from
14 the mainland by a channel some 3 km wide, it is surrounded by reversing tidal streams of up to 4 m s⁻¹
15 ¹ at spring tides. These local hydrodynamic details and their consequences are unresolved by satellite
16 altimetry, nor are they represented in regional tidal models. Here we look at the effects of the island
17 on the strong tidal stream in terms of the budgets for tidal energy dissipation and the formation and
18 shedding of eddies. We show, using local observations and a satellite altimetry constrained product
19 (TPX09), that the island has a large impact on the tidal stream, and that even in this latest altimetry
20 constrained product the derived tidal stream is under-represented due to the island not being
21 resolved. The effect of the island leads to an underestimate of the current speed in the TPX09 data in
22 the channel of up to a factor of 2.5, depending on the timing in the spring-neap cycle, and the average
23 tidal energy resource is underestimated by a factor up to 7. The observed tidal amplitudes are higher
24 at the mainland than at the island, and there is a detectable phase lag in the tide across the island –
25 this effect is not seen in the TPX09 data. The underestimate of the tide in the TPX09 data has
26 consequences for tidal dissipation and wake effect computation and show that local observations are
27 key to correctly estimate tidal energetics around small-scale coastal topography.
28

29 1 Introduction

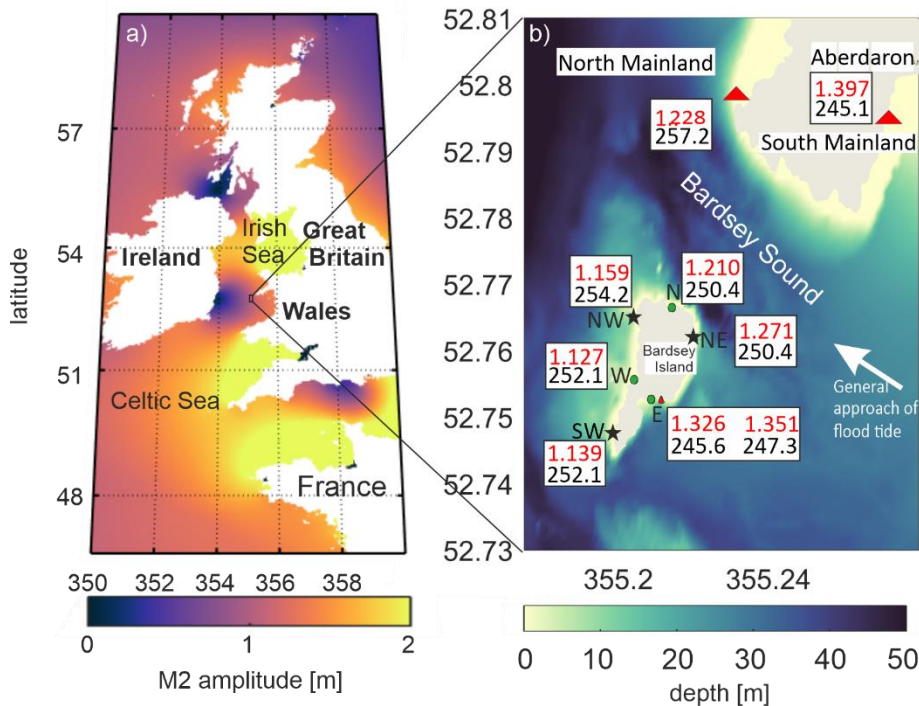
30 Scientific understanding of global tidal dynamics is well established. Following the advent of satellite
31 observations, up to 15 tidal constituents have been mapped using altimetry constrained numerical
32 models, and the resulting products verified and constrained further using *in situ* tidal data – see
33 Stammer et al. (2014) for details. There is, however, still an issue in terms of spatial resolution of the
34 altimetry constrained products: even the most recent (global) tidal models have only $1/30^\circ$ resolution
35 (equivalent to ~ 3.2 km in longitude at the equator, some 1.9 km in the domain here, and 3.2 km in
36 latitude everywhere). The satellite themselves may have track separation of 100s of km (Egbert and
37 Erofeeva, 2002) and the coastline can introduce biases in the altimetry data which limits the usefulness
38 of it in the assimilation process. This means that smaller topographic features and islands are
39 unresolved, and may be “invisible” in altimetry constrained product even if the features may be
40 resolved in the latest bathymetry databases, e.g., the General Bathymetric Chart of the Oceans
41 (GEBCO, <https://www.gebco.net/>; Jakobsson et al., 2020). This can mean that the energetics in the
42 products, and in other numerical model with insufficient resolution, can be biased because the wakes
43 can act as a large energy sink (McCabe et al., 2006; Stigebrandt, 1980; Warner and MacCready, 2014).
44 Whilst the globally integrated energetics of these models is consistent with astronomical estimates
45 from lunar recession rates (Bills and Ray, 1999; Egbert and Ray, 2001), the local estimates can be
46 wrong. However, new correction algorithms improve the satellite data near coasts (e.g., Piccioni et al.,
47 2018), but this is yet to be included in global tidal products.

48
49 Because many of the altimetry constrained tidal database are models, and not altimeter databases,
50 they also provide tidal currents as well as elevations. This is true for TPXO9 (see Egbert and Erofeeva,
51 2002 and <https://www.tpxo.net/> for details), the altimetry constrained product used here. Here, we
52 use a series of tide-gauge measurements from Bardsey Island in the Irish Sea (Figure 1) alongside
53 TPXO9 to evaluate the effect of the island on the tidal dynamics as they track around Bardsey Island.
54 Bardsey Island is a rocky melange of sedimentary and igneous rocks including some granites, located
55 3.1 km off the Llŷn Peninsula in North Wales, UK (Figure 1a). It is approximately 1 km wide, though
56 only 300 m at the narrowest part, and 1.6 km long. It reaches 167 m at its highest point. Bardsey
57 Sound, between the Llŷn peninsula and the island, experiences strong tidal currents. The relatively
58 small scale of the island and the Sound means that the local detail is not “seen” in the altimetry
59 constrained products. The uncaptured, by the altimetry constrained data, active local tidal dynamics
60 allows us to compare the altimetry constrained tidal characteristics in TPXO9 for the region with
61 accurate local observations and quantify the validity limits of TPXO9 for this type of investigation. We
62 will make a direct comparison of the tidal amplitudes and phases measured by the bottom pressure
63 gauges around the island (see Figure 1b for tide gauge (TG) locations and a summary of the *in situ*
64 tides). We also consider whether, and when, in the tidal cycle, flow separation occurs in the wake of
65 the island.

66
67 We will use some basic fluid-flow parameters in our analysis later. Transition to turbulence, and hence
68 flow separation around an object, can be parameterised in terms of a Reynolds number, $Re = UD/\nu$,
69 where U is a velocity scale, D is the size of the object, and $\nu \sim 100$ is a horizontal diffusivity (see, e.g.,
70 Wolanski et al., 1984). It indicates when there is a transition to flow separation behind the island: at
71 low Reynolds numbers, $Re < 1$, the flow is quite symmetric upstream and downstream, and there is no
72 flow separation at the object. As the Reynolds number is increased to the range $10 < Re < 40$, laminar
73 separation happens and results in two steady vortices downstream. As Re increases further, up to
74 $Re < 1000$, these steady vortices are replaced by a periodic von Karman vortex street, whereas if
75 $Re > 1000$, there is a fully separated turbulent flow (Kundu and Cohen, 2002).

76
77 Another useful non-dimensional number for this type of investigation is the Strouhal number, $St =$
78 fD/U . Here, f is the frequency of the shedding of vortices, and fully developed vortices are generated
79 when $T > f$ and T is the frequency of the oscillating flow (Dong et al., 2007; Magaldi et al., 2008). If, on

80 the other hand, the tidal frequency is larger than f only one wake eddy will be shed on each tidal cycle,
 81 if it has time to form at all.
 82



83
 84 Figure 1: a) Map of the European shelf showing M_2 amplitudes in meters, from TPX09.
 85 b) details of local topography and tidal characteristics in the vicinity of Bardsey Island. The symbols
 86 mark the TG location, with green ellipses denoting phase 1, black stars phase 2, and red triangles phase
 87 3. Note that East was occupied twice, during Phases 1 and 3. The red numbers in the text boxes are
 88 the amplitudes (in meters) and the phase lags on Greenwich (in degrees, one degree is almost two
 89 minutes in time) from the harmonic analysis for each tide gauge. The bathymetry comes from
 90 EMODnet (<https://www.emodnet-bathymetry.eu/>).
 91
 92

93 2 Observations

94 2.1 *In situ* data collection

95 The tidal elevations around Bardsey were measured in three phases, from summer 2017 through to
 96 spring 2018 (Table 1 and Figure 1b). Site East, the main harbour for the island at Y Cafn, was occupied
 97 twice as a control, during Phase 1 and 3. The other instrument deployments were bottom mounted a
 98 few tens of metres laterally offshore, and all instruments were deployed in depths between 3.2 m and
 99 16.5 m. The instruments used were RBR pressure recorders with a measurement resolution better
 100 than 0.001 m and they were set to sample every 6 minutes.
 101

102 The resulting pressure series were analysed to extract tides, using the Tidal Analysis Software Kit of
 103 the National Oceanographic Centre (NOC, 2020). Analyses were made for 26 constituents, including
 104 Mean Sea Level, and eight related constituents, appropriate for a month or more of data (Pugh and
 105 Woodworth, 2014). In Table 2 the three constituents listed are the two biggest, M_2 and S_2 , and (as an
 106 indicator of the presence of shallow water tides) M_4 , the first harmonic of M_2 . These shallow water
 107 effects are enhanced around the island because of curvature on the directions of current flow. The
 108 non-tidal residuals, the final column in Table 1, compare well with the residuals at Holyhead, the
 109 nearest permanent tide gauge station some 70 km north; for Holyhead these were 0.096 m, 0.172 m,
 110 and 0.067 m for the same periods (note that bottom pressure measurements at Bardsey include a
 111 partial natural sea level compensation for the inverted barometer effect). Phase 2 residuals at Bardsey

112 and at Holyhead, were noticeably higher than the other two phases because Phase 2 included one of
 113 the most severe storms and waves in local memory: hurricane Ophelia, which had maximum local
 114 wind speeds on 16 October 2017. A good indication of the internal quality of the *in situ* observations
 115 and analyses is given by the consistency in the tidal ages and S_2/M_2 amplitude ratios. The tidal age is
 116 the time after maximum astronomical tidal forcing and the local maximum spring tides, or
 117 approximately the phase difference between the phases of S_2 and M_2 in hours, whereas the amplitude
 118 ratios are related to the spring-neap amplitude cycle. These are given in the final columns of Table 2.
 119 The effects of the storm were not noticeable in the tidal signals, as they were at very different natural
 120 frequencies. The subsurface pressure measurements at Bardsey include atmospheric pressure
 121 variations, and any tidal variation therein. However, at these latitudes the atmospheric pressure S_2
 122 variations are very small. At the equator the atmospheric S_2 has an amplitude of about 1.25 mb, which
 123 decreases away from the equator as $\cos^3(\text{latitude})$, so at 53° N the amplitude is reduced to 0.26 mb,
 124 a sea level equivalent of 2.5 mm.

125
 126 Amplitudes and phases of tidal constituents based on short periods of observations need adjusting to
 127 reflect the long-term values of amplitudes and phases. The values in Table 2 have been adjusted for
 128 both nodal effects and for an observed non-astronomical seasonal modulation of M_2 . Standard
 129 harmonic analyses include an automatic adjustment to amplitudes and phases of lunar components
 130 to allow for the full 3.7%, 18.6-year modulation due to the regression of lunar nodes. However, the
 131 full 3.7% nodal modulation is generally significantly reduced in shallow water and shelf seas, so local
 132 counter adjustments are needed. The nodal M_2 amplitude modulation at Holyhead, the nearest
 133 standard port, is reduced to 1.8% (Woodworth et al., 1991). We have used this value in correcting the
 134 standard 3.7% adjustment. The M_4 nodal modulations are twice that for M_2 . The seasonal M_2
 135 modulations are generally observed to have regional coherence, so we have used the seasonal
 136 modulations from 9 years of Newlyn data (in the period 2000-2011). M_4 is not seasonally adjusted,
 137 and S_2 is not a lunar term, so is not modulated nodally. These very precise adjustments are possible
 138 and useful, but overall, as stated in the caption to Table 2, for regional comparisons we assume, slightly
 139 conservatively, confidence ranges of 1% for amplitudes and 1.0 degrees for phases.

140
 141 Table 1: Details of the pressure gauge deployments. Amplitudes are given to three decimal places as
 142 appropriate for the uncertainties, whereas the timing of constituent phases is probably better than
 143 0.5° (1 minute in time for M_2).

Station	Latitude North	Longitude East	Time and date Deployed (GMT) Time dd/mm/year	Time and date Recovered (GMT) Time dd/mm/year	Mean Depth (m)	Non-tidal Standard deviation (m)
Phase 1						
North	52.767	355.213	1605 25/5/17	1400 11/7/17	3.9	0.113
East	52.756	355.207	1557 25/5/17	1350 3/7/17	7.0	0.141
West	52.753	355.202	1045 27/5/17	1128 5/7/17	5.6	0.116
Phase 2						
Northwest	52.765	355.203	0000 1/9/17	1110 27/10/17	6.7	0.156
Southwest	52.748	355.197	0000 1/9/17	1145 30/10/17	7.5	0.154
Northeast	52.762	355.220	0000 1/9/17	1240 30/10/17	5.5	0.150
Phase 3						
East	52.753	355.207	1512 7/09/18	0912 05/10/18	3.2	0.095
South Mainland	52.759	355.275	1348 7/09/18	1024 06/10/18	4.8	0.088
North Mainland	52.781	355.236	1500 7/09/18	1512 10/10/18	16.5	0.083

146

147 2.2 TPX09 data

148 The altimetry constrained product used in this paper is that of the TPX09 ATLAS which is derived from
149 assimilation of both satellite altimeter and tide gauge data (Egbert and Erofeeva, 2002). The resolution
150 is $1/30^\circ$ in both latitude and longitude (3.7 km and 2.2 km at Bardsey). We used the elevation and
151 transport information, and their respective phases, for the M_2 , S_2 , and M_4 constituents. In the
152 following calculations, we approximate the largest tidal current speeds or amplitudes as the sum of
153 the amplitudes of the above three tidal constituents. Of course this is only a crude estimate of the full
154 Highest and Lowest astronomical tides. Note that we are not allowing for M_2 to M_4 phase locking, and
155 the relatively small diurnal tides are ignored. We refer to this as the GA (Greatest Astronomical) in the
156 following.

157

158 2.3 LANDSAT data

159 Landsat-8 data images were used to identify possible eddies in the currents and further illustrate
160 unresolved effects due to the island. Note that we are not aiming for a full wake description in this
161 paper. Data were downloaded from the Earth Explorer website (<https://earthexplorer.usgs.gov/>).
162 True colour enhanced RGB images were created with SNAP 7.0 (Sentinel Application Platform;
163 <https://step.esa.int/main/toolboxes/snap/>) using the panchromatic band for red (500 - 680nm, 15m
164 resolution), band 3 for green (530 - 590nm, 30m resolution) and Band 2 for blue (450 - 510 nm, 30m
165 resolution). The blue and green bands were interpolated using a bicubic projection to the 15m
166 panchromatic resolution, and brightness was enhanced to allow easier visualization of the wakes. The
167 images used were taken between 11:00 and 12:00 UTC, when the satellite passed over the area, and
168 the two images were the only cloud-free ones during the measurement periods that were on different
169 stages of the tide.

170

171

172 3 Results

173 3.1 *In situ* Observations

174 The results of the tidal harmonic analyses are shown in Table 2. A spring-neap cycle of parts of the
175 data from the East and West gauges in Phase 1 is plotted in Figure 2 and show a tidal range surpassing
176 4 m at spring tide. Note that the diurnal constituents are not discussed further due to their small (<0.1
177 m) amplitudes. The TG data show M_2 amplitudes of 1.210 m (North), 1.347 m (East) and 1.139 m
178 (West, see Table 2). These give pressure gradients around the island. The narrowest part of the island,
179 some 300 m separates the East and West sites. Here, across-island difference in amplitude give, on
180 spring tides a level difference across 300 m of up to 0.5 m. There is also 6.5° (13 minutes) phase
181 difference for M_2 across the island between the east and the west, with the east leading, consistent
182 with the tide approaching the island from the south and east and then swinging north and east around
183 the Llŷn Peninsula headland. Figures 2b-c show the across island level difference plotted against the
184 measured level at East for two representative days of spring and neap tides. Obviously, the differences
185 are smaller for neap tides. The plots show that the East levels are some 0.5 metres higher in the East
186 than on the West, at High Water on spring tides. On neaps the excess is only about 0.3 m. The
187 differences on the ebb tide are slightly reduced, probably because the direction of flow is partly along
188 the island, steered by the Llŷn Peninsula.

189

190 We do not have access to any current measurements from the region, but the tidal stream is known
191 to reach up to 4 m s^{-1} in the Sound (Colin Evans, pers. comm., and Admiralty, 2017). There is also a
192 simple interpretation of the differences in level across the island from East to West, which indirectly
193 gives approximate values for the wider field of current speeds, which we term, but only in a local
194 sense, the “far-field” currents. Suppose as an island blocking the tidal stream, and ignoring any side
195 effects, the pressure head across the island is given solely by the loss of kinetic energy in the flow, by
196 applying the Bernoulli equation (e.g., Stigebrandt, 1980). The same approach applies for wind forces

197 on an impermeable fence or wall, and the sea level difference, Δh , between East and West is then
 198 given as,
 199

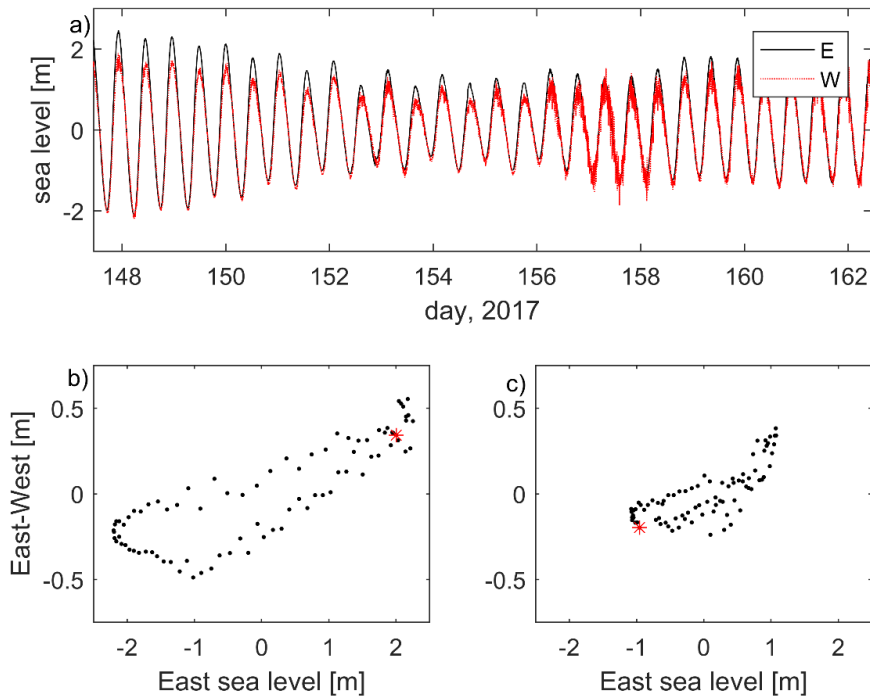
$$200 \quad \Delta h = \frac{v^2}{2g} \quad (1)$$

201
 202 Here, v is the “far field” tidal current speed and g the gravitational acceleration. Then we may indirectly
 203 compute the “far field” tidal currents from the difference in levels across from East to West as the tide
 204 approaches the island (see Figure 1 for the direction of the oncoming tide). Figure 3 a and b (brown
 205 curves) shows the currents so computed, for Day 147 (spring tides) and Day 154 (neap tides), with the
 206 speeds are in metres per second. The blue curves are the measured levels at East. The computed “far-
 207 field” currents have a maximum over 3 m s^{-1} at springs and around 2 m s^{-1} at neaps, similar to local
 208 estimates (Colin Evans, pers. Comm.). The noise in the level differences, shown as currents, (black
 209 curves) may be an indication of turbulence and eddies discussed further below.

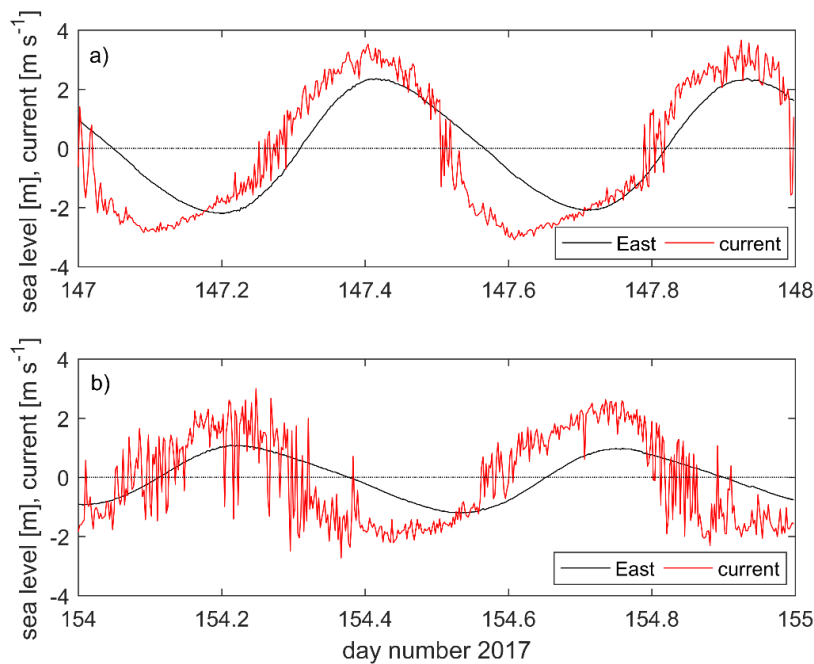
210
 211
 212 Table 2: Results of the tidal (TASK) harmonic analyses. “H” is amplitude (in m) and the phases “G”
 213 (degrees relative to Greenwich) are given in italics. The TPXO9 data was interpolated to the TG
 214 locations and the resulting data given to 0.01 m. The *in situ* RBR data results are given to 0.001 m and
 215 1.0 degrees. However, for regional comparisons we assume confidence ranges of 1% for amplitudes
 216 and 1.0 degrees for phases. RBR constituents are adjusted for nodal and seasonal variations.

		M2		S2		M4		Tidal Age	M2/S2
Station		TG	TPXO	TG	TPXO	TG	TPXO	(hours)	ratio
PHASE 1									
North	H	1.210	1.17	0.458	0.45	0.114	0.12		0.378
	G	<i>250.4</i>	<i>254.4</i>	<i>287.1</i>	<i>287.3</i>	<i>21.7</i>	<i>32.4</i>	<i>36.66</i>	
East	H	1.326	1.16	0.514	0.42	0.147	0.12		0.387
	G	<i>245.6</i>	<i>253.8</i>	<i>283.4</i>	<i>286.7</i>	<i>49.7</i>	<i>34.3</i>	<i>37.76</i>	
West	H	1.139	1.15	0.434	0.42	0.138	0.12		0.381
	G	<i>252.1</i>	<i>253.7</i>	<i>288.4</i>	<i>286.6</i>	<i>36.1</i>	<i>34.8</i>	<i>36.26</i>	
PHASE 2									
NW	H	1.159	1.16	0.431	0.42	0.132	0.12		0.372
	G	<i>254.2</i>	<i>254.7</i>	<i>287.1</i>	<i>287.6</i>	<i>36.4</i>	<i>33.4</i>	<i>32.88</i>	
SW	H	1.217	1.15	0.461	0.42	0.09	0.12		0.379
	G	<i>251.2</i>	<i>253.4</i>	<i>285.5</i>	<i>286.3</i>	<i>27.4</i>	<i>35.6</i>	<i>34.28</i>	
NE	H	1.271	1.15	0.482	0.43	0.096	0.12		0.379
	G	<i>250.4</i>	<i>253.8</i>	<i>284.0</i>	<i>286.7</i>	<i>44.0</i>	<i>32.8</i>	<i>33.58</i>	
PHASE 3									
East	H	1.351	1.16	0.522	0.42	0.138	0.12		0.386
	G	<i>247.3</i>	<i>253.8</i>	<i>282.8</i>	<i>286.7</i>	<i>55.0</i>	<i>34.3</i>	<i>35.5</i>	
S. Mainland	H	1.397	1.21	0.538	0.44	0.152	0.14		0.385
	G	<i>245.1</i>	<i>251.5</i>	<i>280.7</i>	<i>284.4</i>	<i>51.7</i>	<i>37.1</i>	<i>35.6</i>	
N. Mainland	H	1.228	1.2	0.461	0.43	0.074	0.12		0.375
	G	<i>257.2</i>	<i>254.6</i>	<i>290.4</i>	<i>287.6</i>	<i>40.8</i>	<i>29.1</i>	<i>33.2</i>	

217
 218



219
 220 Figure 2: a: Part of the East (black) and West (red) data series, for the in situ data from Phase 1,
 221 covering one spring-neap cycle (arbitrary datums). b and c: Plots of the East-West elevation difference
 222 vs. the elevation at East for springs (b, day 147) and neaps (c, day 154). The red stars show the data
 223 point for 0000 hours on the day. The progression is clockwise.
 224



225
 226 Figure 3: a) Computed current speeds for spring tides, Day 147 (27 May) 2017 in metres per second
 227 (red) compared with the total sea levels at East (in metres, black). The computed currents curve is
 228 noisy as the differences (E-W) are small. The phase relationship between currents is close to a
 229 progressive wave, but with the current maximum to the northwest slightly in advance of the tidal high
 230 water.
 231 b) as in a), but for neap tides on day 154 (4 June) 2017
 232

233 Along the island the differences between Southwest and North are only a few millimetres for M_2 ,
234 within the confidence limits on the analyses. This curvature of the streamlines as the flow is squeezed
235 through Bardsey Sound and swings up around the peninsula, leads to the enhanced generation of non-
236 linear higher tidal harmonics due to curvature on the reversing tidal stream curves. This contributes
237 to the large M_4 amplitudes around the island and headland (Table 2).
238
239

240 3.2 Comparison with TPXO9 data

241 We turn now to a comparison of the tidal analysis data for M_2 from the two sources (see Table 2 for
242 details). When the TPXO9 M_2 data, which has no Bardsey island representation, is interpolated linearly
243 to the TG positions, the result is only a 0.02 m and 0.7° amplitude and phase difference for the Phase
244 1 locations. Compared to the 0.19 m amplitude difference and 6.5° phase difference in the TG data, it
245 is obvious that there is a substantial deficiency in the TPXO9 model in representing the role of the
246 island due to its limited resolution. These results are supported by the Phase 2 measurements (Table
247 2). Phase 3 saw an extended and different approach to the data collection. We revisited East, but also
248 deployed two gauges on the Llŷn peninsula, on the approach to the island (South Mainland)), and
249 north of it (North Mainland). At South Mainland, TPXO is again underestimating the tidal amplitude
250 by more than 10%. At North Mainland, some 5 km north of Bardsey, and just north of the Sound,
251 however, the TG and TPXO amplitudes are within 1 cm of each other. This again shows the effect
252 Bardsey and local topography have on the tidal amplitudes in the region.
253

254 As a representation of the shallow-water tidal harmonics, the TPXO M_4 amplitude agrees well with the
255 TG data at North (0.12 and 0.11 m, respectively), but overestimates the amplitude at North Mainland
256 (0.07 m in the TG data and 0.12 m from TPXO; see Table 2). Because higher harmonics are generated
257 locally by the tidal flow itself, this again shows the effect of the island on the tidal stream; the M_4
258 amplitude is halved along Bardsey Sound in the TG data, whereas TPXO overestimates it and shows
259 only minor variability. The overestimate in TPXO can lead to the tidal energetics being biased high in
260 the region if they are based on the that data alone.
261

262 This is illustrated in the TPXO9 spring and neap flood currents in Figure 4a-b, and the magnitude of
263 the current in the Sound in Figure 4c. These currents are weaker than the far field estimate using Eq.
264 (1) above. For spring tides, TPXO9 shows a current of up to 1.5 m s^{-1} in the Sound and 2.5 m s^{-1} in the
265 far field, whereas the TG data and Eq. (1) comes out at 3.7 m s^{-1} from Eq. (1) for the spring tide far
266 field (*cf.* Figures 3 and 4). For neaps the corresponding values are 0.6 m s^{-1} in the Sound and 1.5 m s^{-1}
267 in the far field from TPXO9, and 3.0 m s^{-1} from the TG data and Eq. (1). The local sea-going experts
268 (Colin Evans, pers. comm.) and the Admiralty chart for the Sound (Admiralty, 2017) state a current
269 speed of up to 4 m s^{-1} , so TPXO9 underestimates the currents in the strait with a factor ~ 2.5 , whereas
270 the observations, even under the assumptions behind Eq. (1), get within 10%. One can argue that the
271 sea-level difference along the strait will lead to an acceleration into the strait as well (see e.g.,
272 Stigebrandt, 1980), that could be added to the far field current. However, frictional effects will come
273 into play and a large part of the along-strait sea level difference will be needed to overcome friction
274 and form drag (Stigebrandt, 1980). In fact, of the 0.32 m GA sea-level difference between South and
275 North Mainland (see Table 1), only 0.006 m is needed to accelerate the spring flow from 3.66 to 4 m s^{-1}
276 in Eq (1). That means that almost the complete sea-level different along the strait is due to energy
277 losses.
278
279

280 3.3 Dissipation

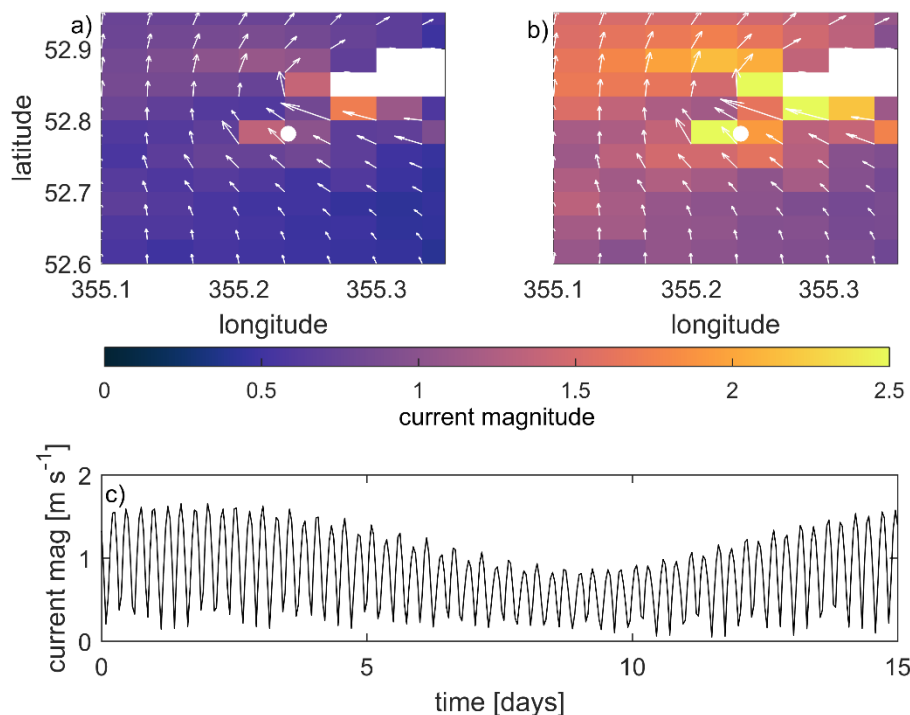
281 To first order, dissipation can be computed from the TPXO9 speed and from the observed amplitude
282 drop along the Sound by comparing the tidal energy flux, E_f , between the two locations. A decrease in
283 the energy flux between two locations can be associated with local dissipation of tidal energy as the

284 wave propagates them (see e.g., Green et al., 2008). The flux of tidal energy is given by (e.g., Phillips,
 285 1977)

286
$$E_f = 0.5c_g\rho gH^2 \quad (3),$$

287 where H is again the tidal amplitude and $c_g = \sqrt{gh}$ is the speed of the tidal wave (h is the water depth
 288 in the Sound, taken to be 37 m), and $\rho=1020 \text{ kg m}^{-3}$ is a reference density. The dissipation, ε , is then
 289 the difference in energy flux between the two mainland TG locations, or $\varepsilon = 0.5c_g\rho g(H_{SM}^2 - H_{NM}^2)$,
 290 taking c_g constant because h changes little between the TG locations. Using the TG amplitudes, the GA
 291 tide would then dissipate 119 kW m^{-1} . Over the 3.1 km width of the Sound, this integrates to 368 MW.
 292 The M2 tide contributes 31% of this, or 131 MW. This is approximately 0.06% of the 180 GW of M₂
 293 dissipation on the European shelf (see Egbert and Ray, 2000), and is a reasonable estimate for such an
 294 energetic region. Note that this method is independent of the phases between the locations, nor does
 295 it depend on the phases between the amplitudes and currents.

296
 297 The dissipation in a tidal stream can also be computed from $\varepsilon = \rho C_D |u|^3$, where $C_D \sim 0.0025$ is a drag
 298 coefficient (Taylor, 1920). Using the TPX09 current speed in the strait, assuming the Sound to be 3.1
 299 km wide and 2 km long, the GA spring dissipation comes out as 53 MW (using $u=1.5 \text{ m s}^{-1}$), and the M₂
 300 dissipation (using a current speed of 1.2 m s^{-1}) as 28 MW. This is a substantial underestimate compared
 301 to the estimates above (factors of 7 and ~ 4.5 for the GA and M₂ tides, respectively), which again
 302 highlights the importance of resolving small-scale topography in local tidal energy estimates, and the
 303 use of direct observations in coastal areas to constrain any modelling effort. This dissipation here is
 304 only a small fraction of the European Shelf and coastline, but it is a very energetic area. Although the
 305 Bardsey tides are unusually energetic, underestimated local coastal energy dissipation may be
 306 substantial in the TPX09 (and similar) data and numerical models.



307
 308 Figure 4: The current magnitude (colour) and vectors at spring (a) and neap (b) flood tides from TPX09.
 309 These are computed from the M2 and S2 constituents only. The white circle shows the location of
 310 Bardsey – note that it is not resolved in the TPX09 data and has been added for visual purposes only.
 311 c) The magnitude of the tidal current during a spring-neap cycle in the Sound using the M2, S2, and
 312 M4 constituents in the TPX09 data.

313
 314

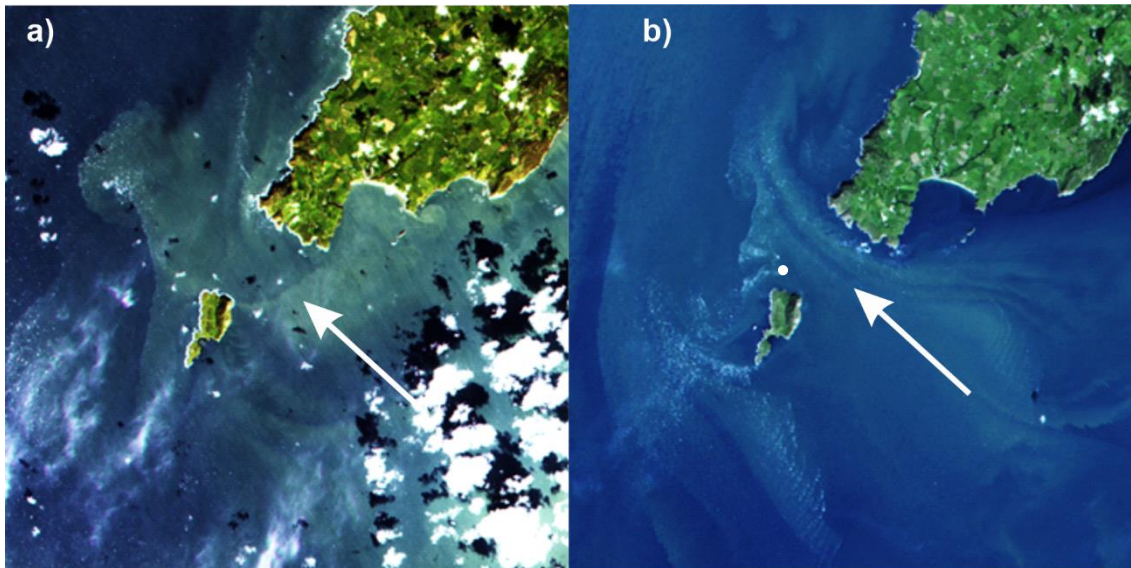
315 3.4 Caveat Emptor!

316 We have shown above that the tidal elevations are underestimated in the TPX09 data, and that the
317 current magnitude is most likely underestimated as well, so our computations of the energetics and
318 non-dimensional numbers are conservative. The two extremes in tidal current magnitude in Bardsey
319 Sound can be taken to be the neap tide speed from TPX09 and the astronomic speed computed using
320 TG data and TPX0 combined. We thus have 0.9 m s^{-1} (neaps from TPX09, not discussed above) as the
321 lower range, and 4 m s^{-1} (astronomic computed) as the upper estimate.

322
323 Even using the much-underestimated current speeds from the TPX0-data, the indications are that
324 there would be no stratification locally. The Simpson-Hunter parameter is $X = h/u^3 \approx 70$ for Bardsey
325 Sound (Simpson and Hunter, 1974). This means that the area is vertically mixed due to the tides alone.
326 The eddies shed from the island will add more energy to this, further breaking down any potential
327 stratification from freshwater additions (the Simpson-Hunter parameter is based on heat fluxes only)
328 and act to redistribute sediment. The associated Reynolds number for the Island, $Re=UD/\nu$, then
329 comes out at approximately 10 for the neap flow, or approximately 40 for the astronomic tidal current
330 (using $D=1000 \text{ m}$ as the width and $\nu=100 \text{ m}^2 \text{ s}^{-1}$ as the eddy viscosity). This implies laminar separation
331 into two steady vortices downstream of the Island at peak flows, and the vortices can be expected to
332 appear on both ebb and flood flows (Edwards et al., 2004; Wolanski et al., 1984). There may not be
333 any vortex shedding during neap flows, however, because $Re \sim 10$.

334
335 The Strouhal number $St = fL/U$, is typically about 0.2 for the Re numbers found here (Wolanski et al.,
336 1984), giving $f=St U/L = 0.2U/1500 \Rightarrow 1 \times 10^{-4} < f < 5 \times 10^{-4}$ and an associated vortex shedding period of
337 3-17 hours ($L=1500\text{m}$ is the length of the island). This means that fully developed eddies can be
338 generated at the higher flow rates, because our tidal period (12.4 hours) is longer than the vortex
339 shedding period a few hours). However, at neap flows there is no time to develop a fully separated
340 vortex within the timeframe of a tidal cycle.

341



342
343 Figure 5: Landsat 8 images from October 5, 2017 (a) and September 13, 2018 (b). The tidal phases are
344 halfway through the tidal cycle on the neap flood in a) and just after spring high tide in b). The white
345 dot north of the island in panel b) is an exposed rock generating a second wake. See
346 <https://landsat.gsfc.nasa.gov/data/> for data availability.

347

348 This conclusion is supported by satellite images from Landsat 8 (Figure 5), which shows a very different
349 picture between neaps (Figure 5a) and springs (Figure 5b). At spring tides, there are two clear wakes

350 behind the tips of the island (marked with arrows), whereas at neaps (Figure 5a) there is only a more
351 diffuse image in Bardsey Sound, and no signal of a wake behind the south tip of the island-

352
353

354 4 Discussion

355 This brief account was triggered by an interest in detailed mapping of tides in a reversing tidal stream.
356 The results highlight the effect small coastal islands can have on tides in energetic settings, and they
357 highlight the limitations of altimetry-constrained models near coastlines where the bathymetry used
358 in the model is unresolved. Even though TPXO9, which is used here, is constrained by a series of tide
359 gauges in the Irish Sea, including north and south of Bardsey, the island is some 60 km from the nearest
360 long-term tide gauge (in Holyhead, to the north of Bardsey). Consequently, the tidal amplitudes in the
361 database are not representative of the observed amplitudes near the island, and the currents are
362 underestimated by a factor close to 2.5 for the GA tide. This underestimate also means that wake
363 effects may be underestimated if one relies solely on altimetry constrained models (or coarse
364 resolution numerical models) unable to resolve islands, with consequences for navigation, renewable
365 energy installations, and sediment dynamics.

366
367 Future satellite mission may be able to resolve small islands like Bardsey, and improved methods will
368 allow for better detection of the coastlines. In order to obtain tidal currents, however, one still has to
369 assimilate the altimetry data into a numerical model and it will probably be some time before we can
370 simulate global ocean tides at a resolution good enough to resolve an island like Bardsey.

371
372 The results do have wider implications for, among others, the renewable industry, because we show
373 that local observations are necessary in regions of complex geometry to ensure the energy resource
374 is determined accurately. Using only TPXO9 data, the dissipation – an indicator of the renewable
375 resource – is underestimating the astronomic potential with a factor up to 7 of the real resource. There
376 is also the possibility that wake effects behind the island would be neglected without proper surveys,
377 leading to an erroneous energy estimate. The results also highlight that concurrent sea level and
378 current measurements are needed to fully explore the dynamics and quantify, e.g., further pressure
379 effects of the island on the tidal stream. Consequently, we argue that in any near-coastal investigation
380 of detailed tidal dynamics, the coastal topography must be explicitly resolved, and any modelling
381 effort should be constrained to fit local observations of the tidal dynamics.

382
383

384 **Acknowledgements:** Instrument deployments and recovery were planned and executed with the
385 assistance of the Bardsey ferry operator, Colin Evans, and by Ernest Evans, the local lobster fisherman
386 and expert on Bardsey tidal conditions. The Phase 1 observations were partly funded by the Crown
387 Estate. The Landsat data was processed by Dr Madjid Hadjal and Professor David McKee at University
388 of Strathclyde, and constructive comments from Prof. Phil Woodworth and two anonymous reviewers
389 improved the manuscript.

390
391 **Code/Data availability:** The data is available from the Open Science Framework
392 (https://osf.io/kvgur/?view_only=ff2d8bd12a61493aa1dfa9011ecdde81)

393
394 **Author contributions:** JAMG wrote the manuscript and did the computations. DTP did the
395 measurements, processed the TG data, and assisted with the writing.

396
397 **Competing interests:** The authors declare no competing interest

398
399

400 References

- 401 Admiralty: Cardigan Bay Northern Part,, Chart no. 1971, 2017.
- 402 Bills, B. G. and Ray, R. D.: Lunar orbital evolution: A synthesis of recent results, *Geophys. Res. Lett.*,
403 26(19), 3045–3048, doi:10.1029/1999GL008348, 1999.
- 404 Dong, C., McWilliams, J. C. and Shchepetkin, A. F.: Island Wakes in Deep Water, *J. Phys. Oceanogr.*,
405 37(4), 962–981, doi:10.1175/jpo3047.1, 2007.
- 406 Edwards, K. A., MacCready, P., Moum, J. N., Pawlak, G., Klymak, J. M. and Perlin, A.: Form Drag and
407 Mixing Due to Tidal Flow past a Sharp Point, *J. Phys. Oceanogr.*, 34(6), 1297–1312, doi:10.1175/1520-
408 0485(2004)034<1297:fdamdt>2.0.co;2, 2004.
- 409 Egbert, G. D. and Erofeeva, S. Y.: Efficient inverse Modeling of barotropic ocean tides, *J. Atmos. Ocean.*
410 *Technol.*, 19, 183–204, 2002.
- 411 Egbert, G. D. and Ray, R. D.: Significant dissipation of tidal energy in the deep ocean inferred from
412 satellite altimeter data, *Nature*, 405(6788), 775–778, doi:10.1038/35015531, 2000.
- 413 Egbert, G. D. and Ray, R. D.: Estimates of M2 tidal energy dissipation from Topex/Poseidon altimeter
414 data, *J. Geophys. Res.*, 106, 22475–22502, 2001.
- 415 Green, J. A. M., Simpson, J. H., Legg, S. and Palmer, M. R.: Internal waves, baroclinic energy fluxes and
416 mixing at the European shelf edge, *Cont. Shelf Res.*, 28(7), 937–950, doi:10.1016/j.csr.2008.01.014,
417 2008.
- 418 Jakobsson, M., Mayer, L. A., Bringensparr, C., Castro, C. F., Mohammad, R., Johnson, P., Ketter, T.,
419 Accettella, D., Amblas, D., An, L., Arndt, J. E., Canals, M., Casamor, J. L., Chauché, N., Coakley, B.,
420 Danielson, S., Demarte, M., Dickson, M. L., Dorschel, B., Dowdeswell, J. A., Dreutter, S., Fremand, A.
421 C., Gallant, D., Hall, J. K., Hehemann, L., Hodnesdal, H., Hong, J., Ivaldi, R., Kane, E., Klaucke, I.,
422 Krawczyk, D. W., Kristoffersen, Y., Kuipers, B. R., Millan, R., Masetti, G., Morlighem, M., Noormets, R.,
423 Prescott, M. M., Rebesco, M., Rignot, E., Semiletov, I., Tate, A. J., Travaglini, P., Velicogna, I.,
424 Weatherall, P., Weinrebe, W., Willis, J. K., Wood, M., Zarayskaya, Y., Zhang, T., Zimmermann, M. and
425 Zinglensen, K. B.: The International Bathymetric Chart of the Arctic Ocean Version 4.0, *Sci. Data*, 7(1),
426 doi:10.1038/s41597-020-0520-9, 2020.
- 427 Kundu, P. K. and Cohen, I. M.: *Fluid Mechanics*, second edition, Academic Press, San Diego., 2002.
- 428 Magaldi, M. G., Özgökmen, T. M., Griffa, A., Chassignet, E. P., Iskandarani, M. and Peters, H.: Turbulent
429 flow regimes behind a coastal cape in a stratified and rotating environment, *Ocean Model.*, 25(1–2),
430 65–82, doi:10.1016/J.OCEMOD.2008.06.006, 2008.
- 431 McCabe, R. M., MacCready, P. and Pawlak, G.: Form drag due to flow separation at a headland, *J. Phys.*
432 *Oceanogr.*, 36(11), 2136–2152, doi:10.1175/JPO2966.1, 2006.
- 433 NOC: Tidal Analysis Software Kit, [online] Available from:
434 https://www.psmsl.org/train_and_info/software/task2k.php, 2020.
- 435 Phillips, O. M.: *The Dynamics of the Upper Ocean*, Cambridge University Press, Cambridge, UK., 1977.
- 436 Piccioni, G., Dettmering, D., Passaro, M., Schwatke, C., Bosch, W. and Seitz, F.: Coastal Improvements
437 for Tide Models: The Impact of ALES Retracker, *Remote Sens.*, 10, 700, doi:10.3390/rs1005070, 2018.
- 438 Pugh, D. and Woodworth, P.: *Sea-Level Science*, Cambridge University Press, Cambridge., 2014.
- 439 Simpson, J. H. and Hunter, J. R.: Fronts in the Irish Sea, *Nature*, 250(5465), 404–406,
440 doi:10.1038/250404a0, 1974.
- 441 Stammer, D., Ray, R. D., Andersen, O. B., Arbic, B. K., Bosch, W., Carrère, L., Cheng, Y., Chinn, D. S.,
442 Dushaw, B. D., Egbert, G. D., Erofeeva, S. Y., Fok, H. S., Green, J. A. M., Griffiths, S., King, M. A., Lapin,
443 V., Lemoine, F. G., Luthcke, S. B., Lyard, F., Morison, J., Müller, M., Padman, L., Richman, J. G., Shriver,
444 J. F., Shum, C. K., Taguchi, E. and Yi, Y.: Accuracy assessment of global barotropic ocean tide models,
445 *Rev. Geophys.*, 52(3), doi:10.1002/2014RG000450, 2014.
- 446 Stigebrandt, A.: Some aspects of tidal interaction with fjord constrictions, *Estuar. Coast. Mar. Sci.*, 11,
447 151–166, 1980.
- 448 Taylor, G. I.: Tidal friction in the Irish Sea, *Proc. R. Soc. London Ser. A*, 96, 1–33, 1920.
- 449 Warner, S. J. and MacCready, P.: The dynamics of pressure and form drag on a sloping headland:
450 Internal waves versus eddies, *J. Geophys. Res.*, 119, 1554–1571, doi:10.1002/2013JC009757. Received,

451 2014.

452 Wolanski, E., Imberger, J. and Heron, M. L.: Island wakes in shallow coastal waters, *J. Geophys. Res.*,
453 89(C6), 10553, doi:10.1029/jc089ic06p10553, 1984.

454 Woodworth, P. L., Shaw, S. M. and Blackman, D. L.: Secular trends in mean tidal range around the
455 British Isles and along the adjacent European coastline, *Geophys. J. Int.*, 105, 593–609, 1991.

456